AIAA AVIATION Forum
August 2-6, 2021, VIRTUAL EVENT
AIAA AVIATION 2021 FORUM

10.2514/6.2021-2867

Check for updates

Numerical Detection of Shock Location and Shock Strength in Unsteady Flow Computations

Harsha Rathi* and Krishnendu Sinha†
Indian Institute of Technology Bombay, Maharashtra, India

Shock waves are regions of high gradient in numerical solution of high-speed flows. Numerical methods often have limited accuracy at shock waves. The use of shock sensors becomes vital to identify the shock regions in a flow field and make necessary changes in the numerical methods. Turbulence models used in Reynolds-averaged Navier-Stokes simulations also require modifications at shock waves, and these modifications often depend on the strength of the shock wave. Most of the shock sensors available in the literature predict the shock location, but they do not give any information about the shock properties. In this work, we propose a shock sensor obtained by solving a transport equation that predicts both the location and the strength of a shock in terms of the density ratio across the shock. The shock sensor is validated for a stationary shock and then used in unsteady flow simulation of single-diaphragm and double-diaphragm shock tubes. The sensitivity of the shock sensor to the parameters used in its transport equation, as well as its dependence on grid resolution is studied.

Nomenclature

ρ	=	Density
u	=	Velocity
M	=	Mach Number
t	=	Dimensionless time
x	=	dimensionless distance
ψ	=	instantaneous shock function
ψ_0	=	Reference shock function
ψ_{min}	=	Minimum shock function
l	=	Length scale
dx	=	Grid size
L_ϵ	=	Turbulent length scale
L	=	Characteristic length
a , b	=	Shock sensor constants

I Introduction

Shock waves are an exigent phenomenon associated with high-speed flows, a thin region with very high flow gradients. These large gradients are responsible for high heating, total pressure loss, entropy rise, boundary layer separation, etc. Due to its high compression ability, shock waves are also used as a compression tool for many supersonic or hypersonic engine applications. Computational Fluid Dynamics (CFD) is one of the primary tools for studying the behavior of such high-speed flows using different numerical schemes. However, CFD and numerical schemes being mathematical tool has their own limitations and produce many oscillations near the discontinuity in the final solution. Additional modifications are done to the numerical schemes to achieve a stable solution, but these modifications come at a high computational cost and loss of accuracy. Therefore, accurate detection of shocks in a flow field becomes necessary to get the best possible solution.

*Research Scholar, Department of Aerospace Engineering, IIT Bombay, Powai, Mumbai-400 076
†Professor, Department of Aerospace Engineering, IIT Bombay, Powai, Mumbai-400 076 and AIAA Member.

The thickness of a shock wave is of the order of magnitude of the mean-free path, making shock resolution with numerical method infeasible in most cases of practical interest. In the inviscid limit, shock waves reduce to zero-thickness across which Rankine- Hugoniot jump conditions must be satisfied. Because of the discontinuous nature of shock waves, most standard high-order numerical methods fail in such regions and give large oscillations and errors. Therefore, while simulating such flows, the areas containing shock waves are identified using shock sensors. Then modifications like hybrid schemes, artificial viscosity, and non-linear filtering methods [1, 2] are used in these regions to achieve a smooth, stable solution across such discontinuity. Some shock sensors are used in the post-processing of CFD results also to identify the critical regions [3–5].

There are a number of shock sensors available in literature [1–13]. One of the most widely used shock sensors, Ducros sensor [7] effectively distinguishes between shocks and other compressible turbulence. However, the Ducros sensor is sensitive to dilatation fluctuations in the flow fields where vorticity is negligible. This sensitivity can cause spurious oscillations in the solution, degrading the accuracy and potentially destabilizing the solution. Other unconventional shock sensors like Kanamori sensor [12] use the method of characteristics to identify shock location, which gives accurate results but at a high computational cost. Recently proposed Canny edge shock detection [5] method uses canny edge imaging process to identify shock waves and provides equally accurate results at a comparatively low computational cost. Most of these shock sensors successfully identify shock location, but estimating shock properties accurately and distinguishing between a shock wave and other discontinuities still remains a tough task. Also, great attention is required to construct the computational grid and formulate the sensor to avoid the undefined values that may arise due to the algebraic nature of these sensors.

In the case of flows with shock wave turbulent boundary layer (SBLI) interaction and shock turbulence interaction (STI), the Reynolds-Averaged Navier-Stokes (RANS) simulations yield significant errors in the final solution. Such interactions are highly influenced by mean compression, shock unsteadiness, and entropy fluctuations upstream of the shock. Sinha et al. [14, 15], modeled the shock unsteadiness in the existing $k - \varepsilon$ turbulence model and found it to be a function of upstream shock normal Mach number, i.e., shock strength, which is given as density ratio across the shock. Also, RANS simulations are based on the constant turbulent Prandtl number assumption and give highly inaccurate heat transfer predictions near the shock. This is because the underlying Morkovin's hypothesis breaks in the presence of shock waves. The turbulent Prandtl number is not constant and is a function of shock strength. Due to these reasons, determination of shock strength and shock location becomes essential for accurately simulating flows with SBLI and STI.

Roy et al. [16] proposed a new approach to identify the shock location as well as shock strength at every grid point in terms of a shock function. The shock function is computed by solving a differential equation instead of the algebraic form of other shock sensors. The transport equation of shock function also incorporates a source term that provides an exponential relaxation of its shock value to a pre-defined reference value away from the shock wave. In essence, whenever the transport equation encounters a shock, the shock function changes from its reference value to its shock value, and downstream of the shock, it relaxes back or goes back to its initial reference value exponentially. The shock value of the shock function gives an estimate of the density ratio (shock strength) across the shock wave. The relaxation downstream of shock is necessary to accurately capture multiple shocks in a given flow domain and predict shock strength for each shock. For example, in case of separation shock, reattachment shock, transmitted shock, etc., generated due to boundary layer separation in case of shock impingement on the boundary layer. The length of the domain, shock function takes to go back to its initial reference value from its shock value is called the relaxation length. This relaxation length should be as low as possible to capture multiple shocks in close vicinity to each other accurately. However, the accuracy of density ratio and relaxation length required for exponential relaxation downstream of the shock is highly dependent on each other. If we try to increase the accuracy of obtained shock strength, it will increase the relaxation length exponentially.

In this work, a rigorous study of the one-dimensional form of the transport equation for shock function proposed by Roy et al. [16] is done by applying to one-dimensional unsteady inviscid flows. Some modifications are also made to the original equation to achieve better accuracy in shock strength prediction and relaxation length. Both the original and modified equations are applied to stationary shock for validation and then to unsteady one-dimensional inviscid flow problem in a single diaphragm shock tube and double diaphragm shock tube. The results obtained are then compared to the analytical solution.

II Shock Sensor Equations

The shock function (ψ) transport equation proposed by Roy et al [16] can be written for one dimensional case as:

$$\frac{\partial(\rho\psi)}{\partial t}+\frac{\partial(\rho u\psi)}{\partial x}=\rho\psi\frac{\partial u}{\partial x}-\frac{\rho u(\psi-\psi_0)}{l} \tag{1}$$

where, ψ is the shock function, ψ_0 is the reference value and initial value of shock function across the domain and l is the characteristic length.

Here in equation 1, the left-hand side represents the convection in the shock-normal direction x, the first term on the right-hand side brings in the effect of one-dimensional compression, and the second term results in the exponential post-shock variation. Dropping the last term, and integrating across a stationary shock gives,

$$\frac{\psi_s}{\psi_0}=\frac{u_2}{u_1}=\frac{\rho_1}{\rho_2}=\frac{1}{r} \tag{2}$$

Thus, ψ_s is an indicator of shock strength, and an upstream value of $\psi_0=1$ ensures that we get $\psi_s=1/r$ at the shock location.
Downstream of the shock,

$$\psi=\psi_0+(\psi_s-\psi_0)\exp\left[-\frac{(x-x_s)}{l}\right] \tag{3}$$

Therefore, $\psi=\psi_s$ at the shock location x_s and then downstream of the shock, it relaxes back to $\psi_0=1$ exponentially. How fast this relaxation occurs depends on the selection of characteristic length l. A smaller value of l will result in faster relaxation of shock function downstream of the shock.

In the numerical application for steady or unsteady flows, a shock wave is spread over several grid points and not present just at a particular location in the domain due to which shock function (ψ) is also spread over several grid points. Moreover, the exponential relaxation also becomes active from the first grid point of shock. Due to this, the predicted shock strength is less accurate. So, to have maximum possible accuracy, the exponential relaxation should be minimum, i.e., characteristic length l should be maximum possible near the shock. However, it will also result in an increased relaxation length downstream of the shock.

Proposed Modification

A modification to the existing shock function equation is proposed to tackle the problem of relaxation length and shock function accuracy discussed in the previous section. The characteristic length is no longer constant in the modified sensor equation and is instead maximum near the shock and then reduces as it moves away from the shock.

$$\frac{\partial(\rho\psi)}{\partial t}+\frac{\partial(\rho u\psi)}{\partial x}=\rho\psi\frac{\partial u}{\partial x}-\frac{\rho|u|\,(\psi-\psi_0)}{L} \quad ; \quad L=al[1-b(\psi-\psi_0)] \tag{4}$$

where, a and b are constants and $[1-b(\psi-\psi_0)]\geq 1$ because $(\psi-\psi_0)$ is negative across a shock wave.

Here, characteristic length L will be maximum when the magnitude of $(\psi-\psi_0)$ is maximum, i.e., near the shock. Furthermore, L will be minimum when the magnitude of $(\psi-\psi_0)$ is minimum, i.e., away from the shock. For the constant $b=0$, the modified equation becomes the same as the original equation with a characteristic length equal to al.

In this work, the modified shock function equation 4 is solved along with the one dimensional inviscid Euler's equations, and the results so obtained are compared with the original shock function equation 1 results. The governing equations are discretized in a finite volume formulation where the fluxes are computed using standard Lax-Friedrich's scheme. The artificial viscosity used in the scheme is different for each case to have the least possible dissipation maintaining a stable solution without any oscillations near the discontinuity. The differential term present in the shock function equation's source term is computed using the central difference method. The open boundary condition is used at each end of the shock tube problem.

Figure 1, shows the variation of ψ function for a stationary shock located at x = 0 for two different upstream Mach numbers each for two different length scales ($l=dx$ and $l=L_\epsilon$ *). Grid size $dx=0.0149$, and ρ_1 is the value of

*$l=L_\epsilon$ is the turbulent length scale given by $L_\epsilon=k^{1.5}/\epsilon$ where k and ϵ are turbulent kinetic energy and turbulent dissipation rate respectively

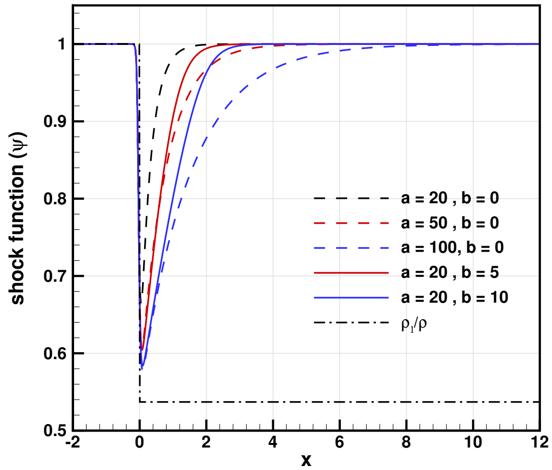

(a) $M = 1.5$**,** $l = dx$

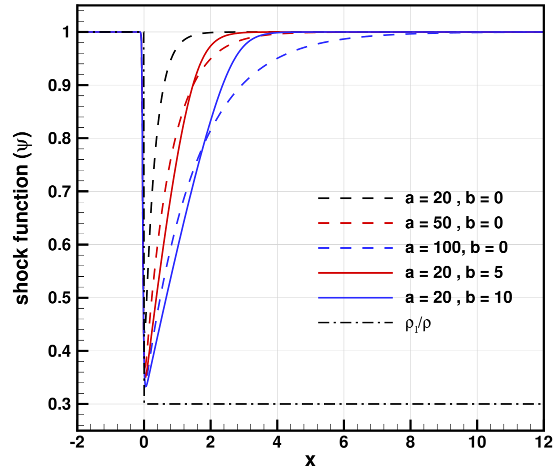

(b) $M = 2.5$**,** $l = dx$

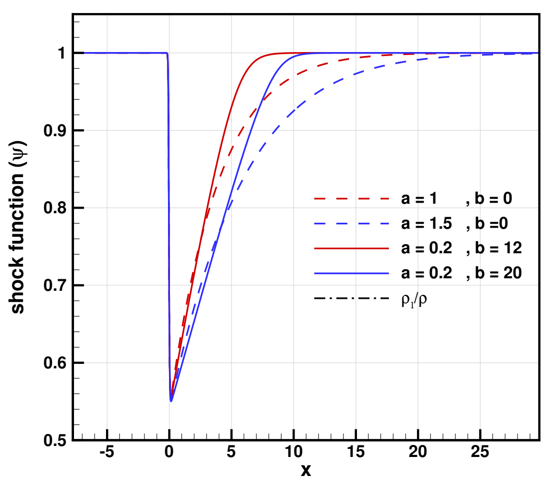

(c) $M = 1.5$**,** $l = L_\epsilon$

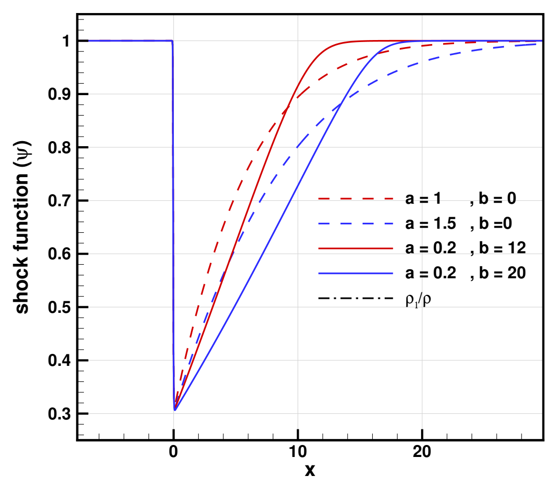

(d) $M = 2.5$**,** $l = L_\epsilon$

Fig. 1 Comparison of original and modified equation for a stationary shock case. Constant $b = 0$ **gives results same as original equation for characteristic length** $= al$**.**

density upstream of the shock. The dotted lines ($b = 0$) shows the results corresponding to the original equation with characteristic length equal to al. The solid lines correspond to the modified equation results for different values b and $a = 20$ for $l = dx$ and $a = 0.2$ for $l = L_\epsilon$. The values for constants a and b are chosen such that ψ_{min} is same for same colored lines for comparing the relaxation length for same minimum value of shock function (ψ_{min}) for original and modified form of the equation. It can be seen that, relaxation length is comparatively less for modified equation case. Another important thing to notice here is that in figures 1a and 1b blue solid line (modified equation with $a = 20$, $b = 10$) have almost same relaxation length as compared to red dotted line (original equation because $a = 20$, $b = 0$) but a more accurate value of ψ_{min}. Similar observation can also be made for $l = L_\epsilon$ case also in figures 1c and 1d.

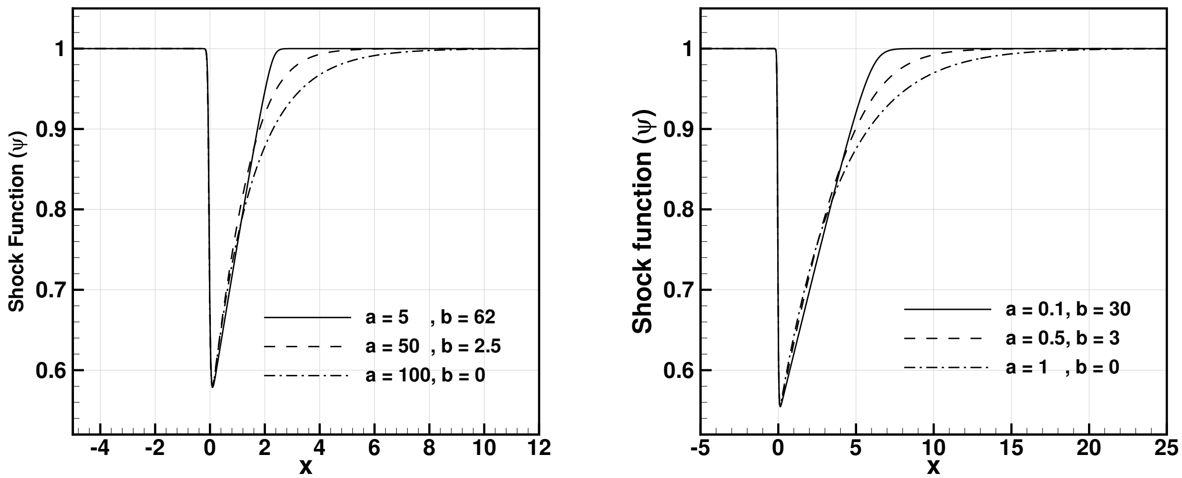

(a) $l = dx$ **(b)** $l = L_\epsilon$

Fig. 2 ψ **Variation for different combinations of** a **and** b **for Mach number M = 1.5. (Note:** ψ_{min} **is same for all cases.)**

a	b	ψ_{min}	**relaxation length**
increases	constant	decreases	increases
constant	increases	decreases	increases
increases	increases	decreases	increases
increases	decreases	depends on amount of change	depends on amount of change

Table 1 **Effect of** a **and** b **on** ψ **variation across a shock for** $l = dx$**.**

Effect of constants a and b

The constants a and b in the modified ψ equation decide the behavior of ψ variation downstream of the shock. Figure 2 shows ψ variation downstream of shock for different a and b values maintaining the same ψ_{min}. The corresponding observations are listed in table 1. For higher values of b, $[1 - b(\psi - \psi_0)]$ can be approximated as $b(\psi - \psi_0)$ near the shock and hence the second term on right hand side in equation 4 reduces to $\rho u/(al)$ i.e. ψ variation can be approximated as linear near the shock. Similarly, if b is small and near 1, the second term on the right-hand side in equation 4 can be approximated as $\rho u(\psi - \psi_0)/(al)$ which will result in exponential variation of ψ downstream of the shock. Therefore, the higher the value of b, the variation of shock function ψ downstream of the shock, will be closer to a linear profile. Similarly, it will be more closer to exponential variation for lower values of b. Therefore, a balance must be maintained between a and b to obtain the optimum variation of shock function downstream of the shock.

III Grid Dependence

Grid dependence was studied for different grid sizes for the uniform grid and exponentially varying grid across a stationary shock of Mach number 1.5 each for two different length scales of $l = dx$ and $l = L_\epsilon$.

Uniform Grid

Figure 3 shows the shock function variation for different grid sizes. Interestingly, the minimum value of shock function (ψ_{min}) does not change with the grid size, but relaxation length decreases exponentially (see fig 3c) with the increase in

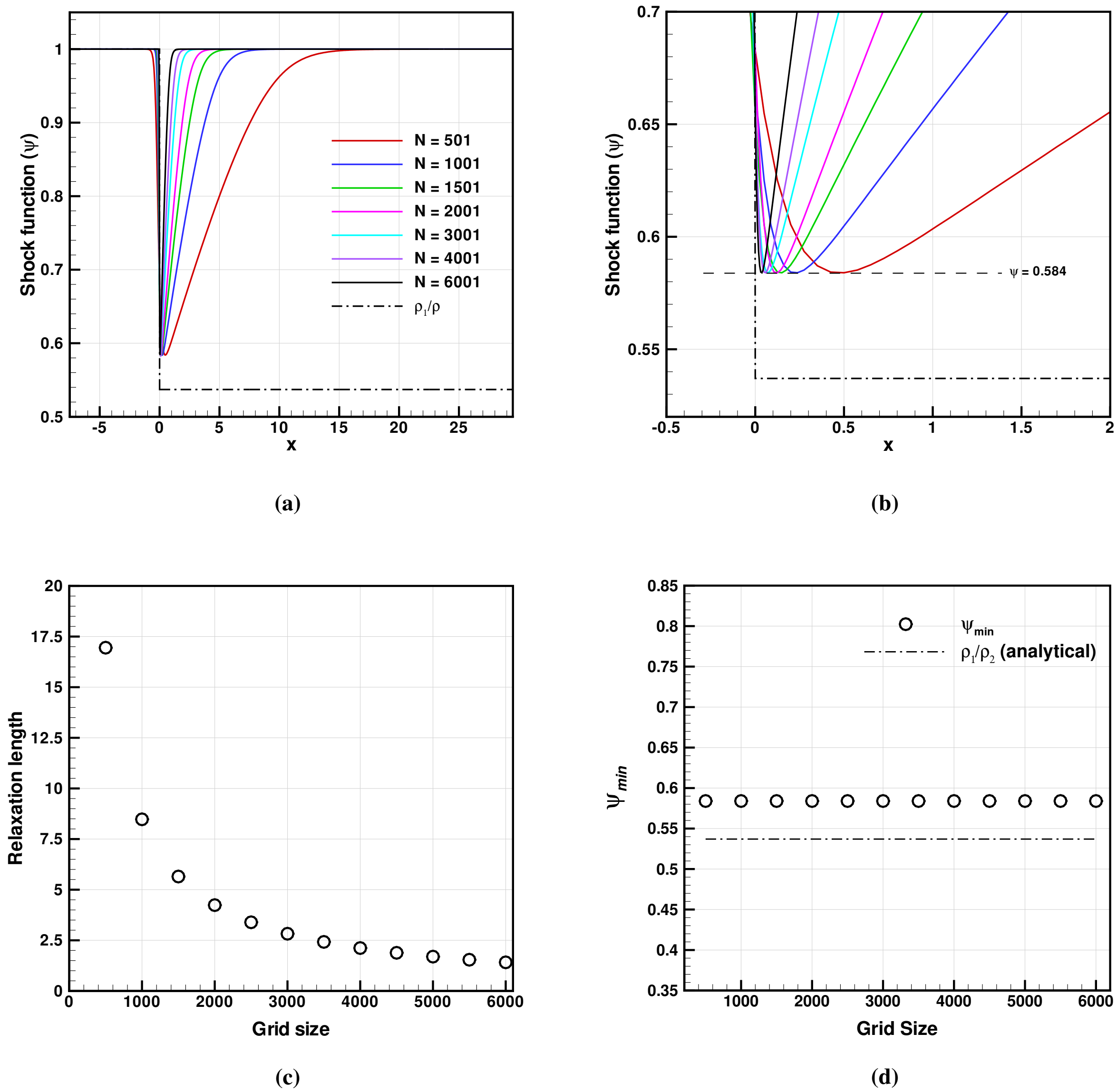

Fig. 3 ψ **Variation for different uniform grid sizes for modified** ψ **equation with** $a = 20$**,** $b = 15$ **and** $l = dx$**.**

the number of grid points. If we observe equation 3 carefully, for a finite grid it can be written as:

$$\psi_2 = \psi_0 + (\psi_1 - \psi_0)\exp\left[-\frac{(x_2 - x_1)}{l}\right] \tag{5}$$

where, ψ_1 and ψ_2 are shock function values at any two locations in the domain x_1 and x_2 respectively.
For $l = Cdx$,

$$\psi_2 = \psi_0 + (\psi_1 - \psi_0)\exp\frac{(n_2 - n_1)}{C} \tag{6}$$

where, n_1 and n_2 are the grid index at location x_1 and x_2 respectively such that $x_1 = (n_1 - 1)dx$ and $x_2 = (n_2 - 1)dx$. From equation 6, it can be observed that the value of ψ is, in fact, dependent on the difference of grid index at any two points of interest. With increase in number of grid points, the dx will reduce and therefore for same $(n_2 - n_1)$

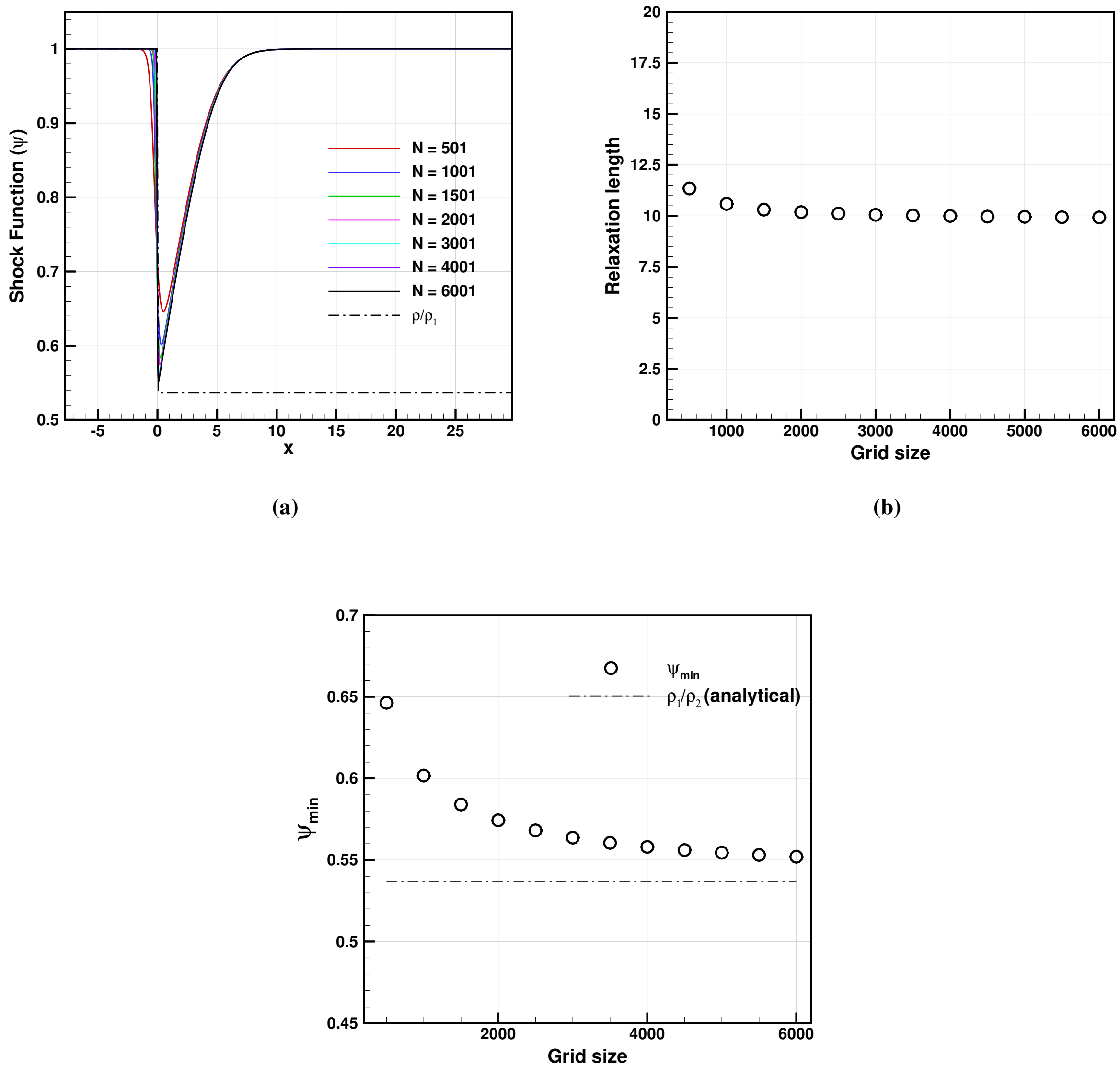

(a) (b) (c)

Fig. 4 ψ Variation for different uniform grid sizes for modified ψ equation with $a = 0.3$, $b = 6$ and $l = L_\epsilon$.

(and corresponding same values of ψ_1 and ψ_2), $(x_2 - x_1)$ will reduce which justifies the reduction in relaxation length. Similar results are observed for modified shock function equation also as shown in figure 3. However, it is a little difficult to see it analytically. In essence, the minimum value of shock function will be the same for all grid sizes for the same value of a and b, but it will be nearer to the shock. The minimum value of shock function can be improved by increasing either one or both of the constants a and b.
For $l = L_\epsilon$,

In the case of turbulent length scale (L_ϵ), observations are quite the opposite to that in the case of dx as length scale. Here, ψ_{min} improves as we move from coarse grid to fine grid, but the relaxation length is almost the same for all cases as seen in figure 4. With grid refinement the ψ_{min} improves because the shock becomes thinner and the effect of exponential increase in shock function value before it reaches its minimum value downstream of the shock is reduced. This result in a more accurate estimation of the ψ_{min}.

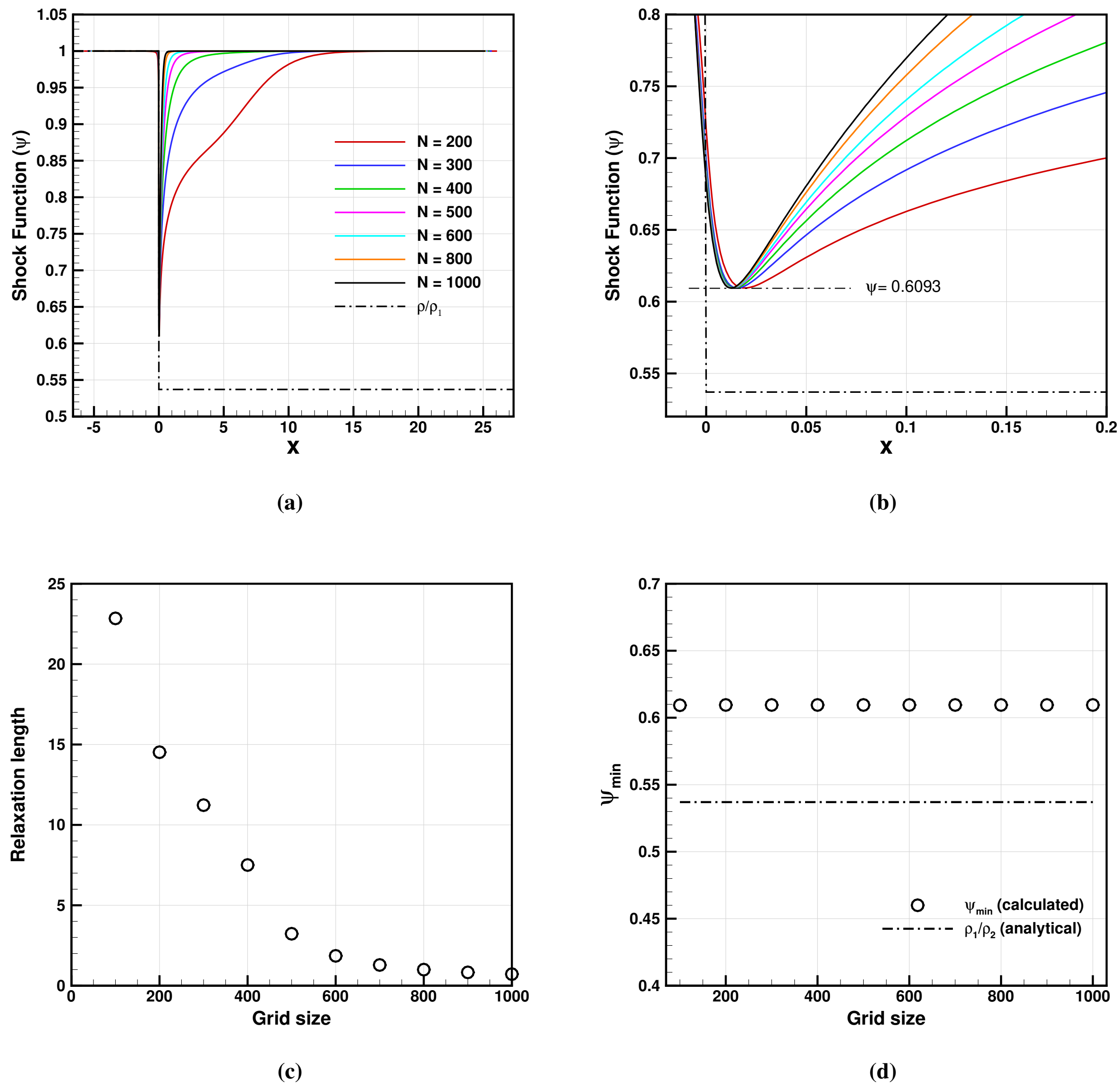

Fig. 5 Shock function (ψ) variation for different exponential grid sizes for modified ψ equation with $a = 20$, $b = 15$ and $l = dx$.

Exponentially stretched grid

For $l = dx$

Figure 5 shows the variation of shock function for $l = dx$ case for different grid sizes with an exponential grid variation with minimum $dx = 10^{-3}$ near the shock at $x = 0$. It can be seen that in this case also, the minimum value of shock function (ψ_{min}) remains independent of grid size and whereas relaxation length varies similar to the case of $l = dx$ with a uniform grid. However, the variation of ψ downstream is not exactly exponential but a little arbitrary. This is because dx is continuously changing with domain length x, and so is the ψ variation per equation 5.

For $l = L_\epsilon$

Figure 6 shows the variation of shock function variation for $l = L_\epsilon$ case for different grid sizes with an exponential grid variation. The dependence of shock function on grid size is similar to that in the case of the uniform grid for $l = L_\epsilon$ case. The ψ_{min} variation here is also almost the same for all grid sizes because of the minimal minimum dx value,

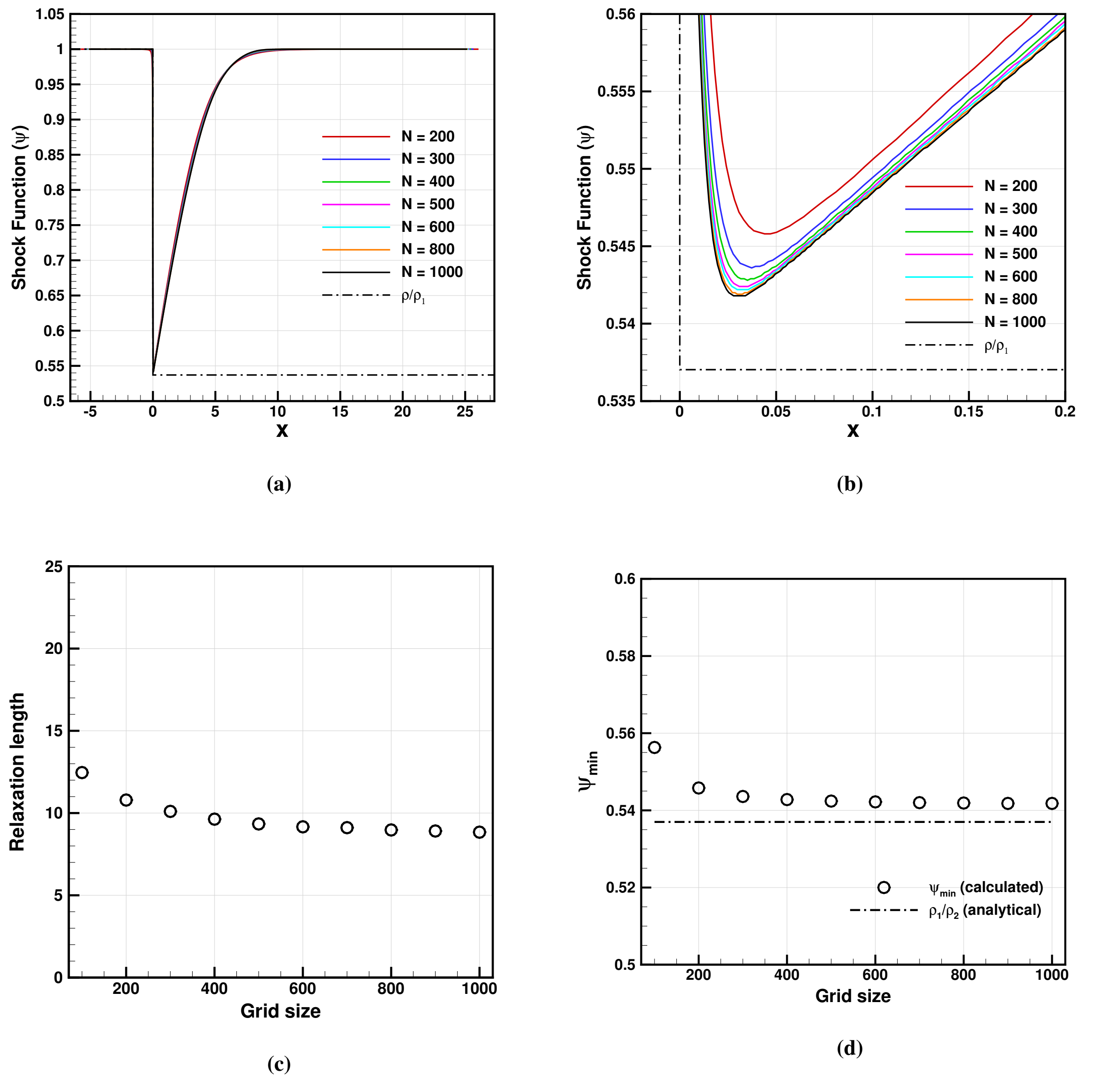

Fig. 6 ψ **Variation for different exponential grid sizes for modified** ψ **equation with** $a = 0.3$**,** $b = 6$ **and** $l = L_\epsilon$**.**

which is already very close to the grid-independent solution.

IV Unsteady Flow Results

In this section, shock sensor results are discussed for two different unsteady flow cases of single diaphragm shock tube and double diaphragm shock tube.

Single Diaphragm Shock tube

A schematic for the shock tube problem is shown in figure 7a. The domain length is from $x = -18.75$ to $x = 18.75$ with diaphragm located at $x = 0$ and a total number of 2500 grid points are used. The initial condition for two different cases

Table 2 Initial gas properties (normalized) for a single diaphragm shock tube.

	Case 1		Case 2	
	State 4	State 1	State 4	State 1
Pressure	5	0.714	10.714	0.714
Temperature	1	1	1	1
Density	7	1	15	1
Velocity	0	0	0	0

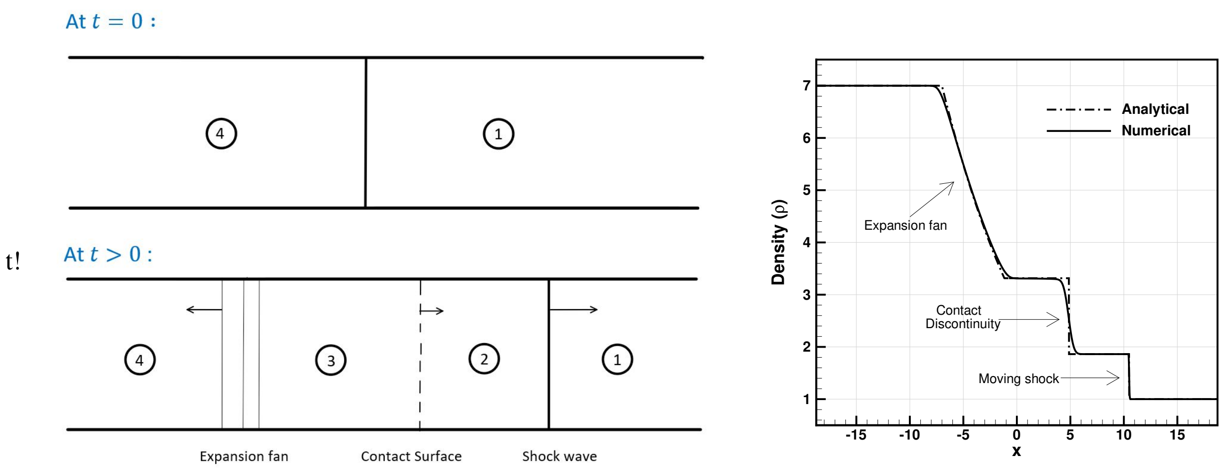

(a) Schematic for a single diaphragm shock tube problem.

(b) Density variation

Fig. 7 (a) Schematic for a single diaphragm shocktube problem and (b) Density variation in a shock tube with diaphragm pressure ratio $(p_4/p_1 = 7)$ **at time** $t = 7$

is listed in table 2. Air at the same temperature and zero velocity are assumed throughout the shock tube for both cases. The density and temperature are normalized with that at state 1. The pressure is normalized with the acoustic dynamic pressure at state 1. The results are plotted for time $t = 7$.

When the diaphragm is ruptured in a shock tube, a shock wave and an expansion wave are generated along with a contact discontinuity separating the two regions. The shock wave moves towards the low-pressure region, and the expansion wave moves toward the high-pressure region. The three different waves can be seen in the density variation plot for the shock tube in figure 7b.

Figure 8 show the results for shock function variation for two different pressure ratios of 7:1 and 15:1. The shock function will have a value less than one and near to shock strength (ρ_1/ρ_2) in the moving shock region. It will have a value greater than 1 in the region of the expansion fan due to positive dilatation (first term in equation 4) in that region. To avoid this, a limiter is used given by $\psi = min(\psi, 1)$. Across a contact surface, velocity is the same and hence zero dilatation; therefore, shock function is not activated in this region and maintains a value equal to ψ_0. The dotted lines in figure 8a and 8b represent the shock function corresponding to original equation with characteristic length $(L = a\ dx)$ and the solid lines represent the modified equation results. The black dash-dot line represents (ρ_1/ρ) and is used as a reference for the accuracy of the minimum shock function value (ψ_{min}) in the shock region. Similar to the stationary shock case, here also modified equation gives better results than the original equation. The relaxation length is comparatively less for the modified equation for the same value of ψ_{min} for both original and modified equation.

Comparison with original equation and analytical results

It is clear that the minimum value of the shock function gives the density ratio across the shock, which can be useful in identifying other shock properties. This minimum shock function value depends on the combination of constants a and b and improves with an increase in either or both constants. Figure 9a shows the variation of ψ_{min} value with b for a

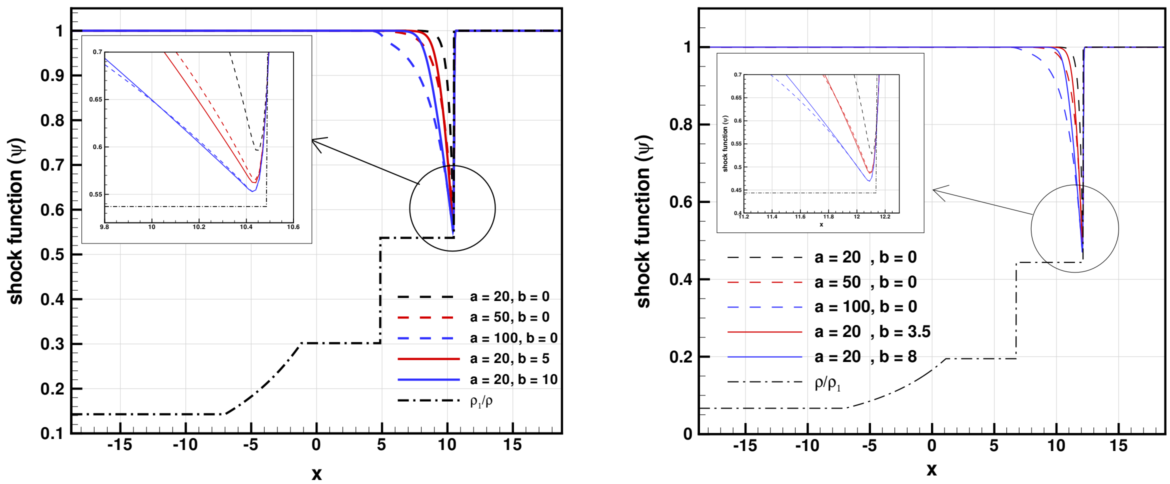

(a) Shock function variation ($p_4/p_1 = 7$) **(b) Shock function variation** ($p_4/p_1 = 15$)

Fig. 8 (a) shock function variation for $p_4/p_1 = 7$ and (b) shock function variation for $p_4/p_1 = 15$ across a shock tube at t = 7.

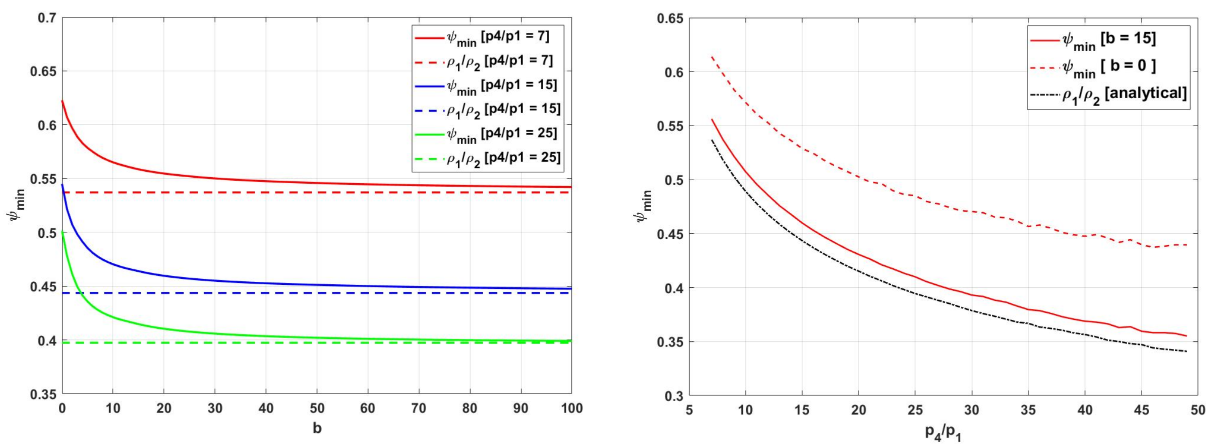

(a) ψ_{min} variation with respect to b **(b) ψ_{min} variation with respect to shocktube pressure ratios.**

Fig. 9 Comparison of estimated ψ_{min} for different values of constant b and diaphragm pressure ratio p_4/p_1 modified and original equation for $l = dx$ and $a = 20$ at $t = 7$ for a single diaphragm shock tube problem.

fixed value of the a for three different pressure ratios for a shock tube. It can be observed that ψ_{min} approaches the analytical value with an increase in constant b. However, it should be noted that with the increase in b for a fixed a, relaxation length for the ψ function downstream of shock will also increase. Figure 9b shows the comparison of original equation ($b = 0$) and modified equation ($b = 15$). The black dash-dot line represents shock strength's analytical value (ρ_1/ρ_2) across a shock generated in a shock tube for different pressure ratios. It can be seen that the modified equation gives a better estimate of shock strength as compared to the original equation.

Double Diaphragm shock tube

For the unsteady flow case of a double diaphragm shock tube, a shock tube with two diaphragm is considered with pressure ratios $p_7 : p_4 : p_1 = 15 : 7 : 1$. A schematic for the same is shown in figure 10a. The domain length is from

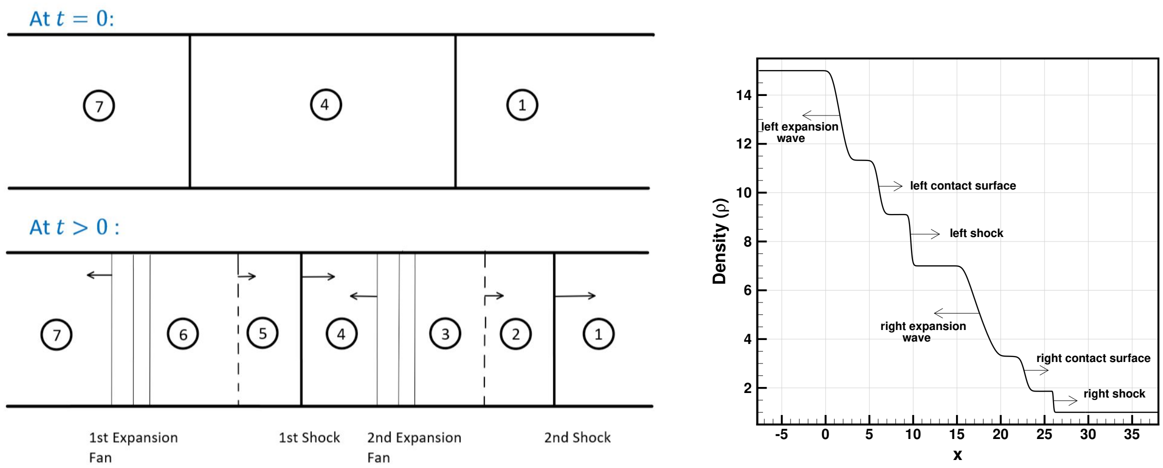

(a) Schematic for a double diaphragm shock tube problem.

(b) Density variation

Fig. 10 (a) Schematic for a double diaphragm shocktube problem and (b) Density variation for a double diaphragm shock tube case for diaphragm pressure ratio $15 : 7 : 1$ **showing different waves at time** $t = 4$**.**

$x = -7.6$ to $x = 122.6$ with two diaphragm located at $x = 5$ and $x = 20$. A total number of 4200 grid points are used for simulations with the following initial conditions:

$$p = \begin{cases} 10.714, & \text{if } x < 5 \\ 5, & \text{if } 5 < x < 20 \\ 0.714, & \text{if } x > 20 \end{cases} \qquad \rho = \begin{cases} 15, & \text{if } x < 5 \\ 7, & \text{if } 5 < x < 20 \\ 1, & \text{if } x > 20 \end{cases}$$

Air at same temperature and zero velocity are assumed throughout the shock tube at time $t = 0$.

In a double diaphragm shock tube problem, when both the diaphragms are ruptured at the same time, two right moving shocks (left shock generated from left diaphragm at $x = 5$ and right shock generated from right diaphragm $x = 20$). Two left moving expansion waves, and two right moving contact surfaces are generated respectively from the two diaphragms. Figure 10b shows the density variation for this case at $t = 4$. The arrows show the directions of the respective waves. Now two normal shocks cannot exist in a single one-dimensional domain, and hence, the left shock will try to catch up with the right shock and eventually form a single stronger moving shock. During this process, the left shock will pass through the right expansion wave, moving in the opposite direction. It will also cross the right contact surface, which is moving in the same direction. Hence, the flow conditions upstream of the left shock will be different at different stages of the flow, which might affect the properties of both the shocks like shock strength and shock speed.

Figure 11 shows ψ variation for the double diaphragm shock tube problem at different time steps. It can be seen that the shock function (ψ) identifies the shock location for both the shocks. It does not detect the expansion fan and contact discontinuity region. The shock function's negative peaks at two locations give an estimate of the shock strength for both the shocks. The ψ_{min} for the left shock is higher than that of the right shock, which signifies that the left shock is weaker than the right one. This is because the diaphragm pressure ratio ($p_7/p_4 = 15/7 = 2.143$) is lower than that across the right diaphragm ($p_4/p_1 = 7$) and hence the right diaphragm produces a stronger shock. As time progresses, it can be noticed that the left shock moves faster than the right shock. It passes through right expansion fan (figure 11b), then through the right contact discontinuity (figure 11c) and eventually meets up with the right shock (figure 11e) and then moves forward as a stronger shock (figure 11f).

Figure 12 shows the variation of ψ_{min} with time for both the shocks. The two domes in ψ_{min} variation for the left shock marks the passing of left shock through the right expansion wave and right contact discontinuity. At around $t = 47$, both the shocks meet and move forward as a stronger shock with a lower ψ_{min}. It can be observed that ψ_{min} for left shock reduces gradually with time over a difference of around 6 to 8 time units. However, in reality, the meeting of the two shocks and forming stronger shock will be instantaneous, with the time taken to be infinitesimally small. This discrepancy is due to the relaxation length required by the shock function to go from its minimum value ψ_{min} at the shock to its reference value of ($\psi_0 = 1$) downstream of the shock. When the left shock approaches the right shock, and

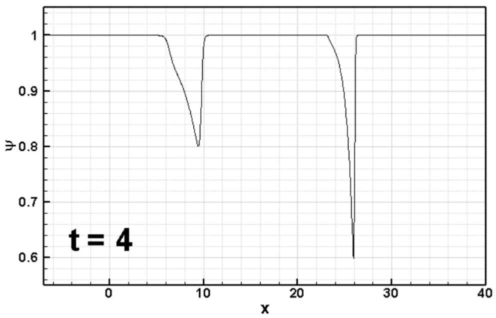

(a) ψ **Variation at** $(t = 4)$

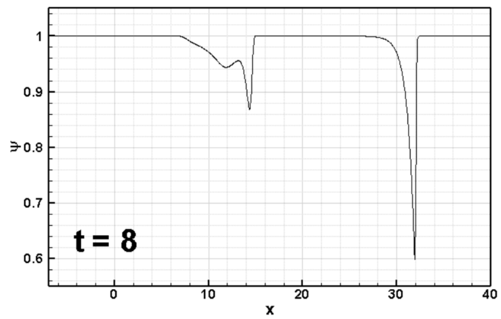

(b) ψ **Variation at** $(t = 8)$

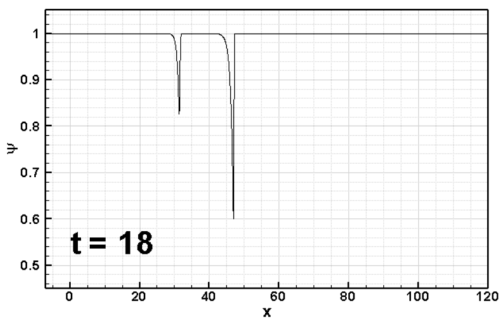

(c) ψ **Variation at** $(t = 18)$

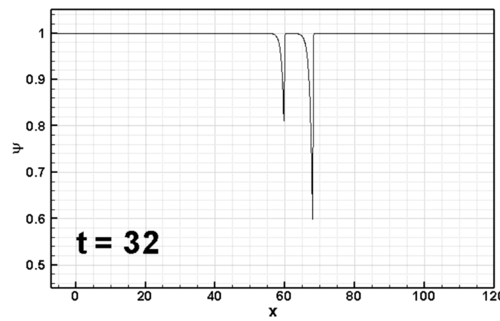

(d) ψ **Variation at** $(t = 32)$

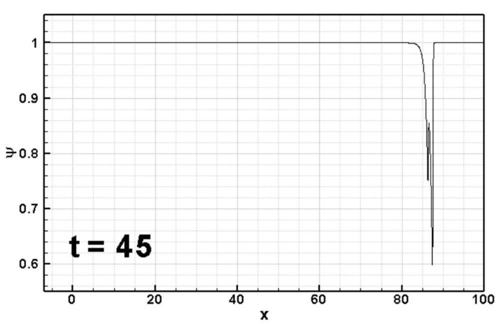

(e) ψ **Variation at** $(t = 45)$

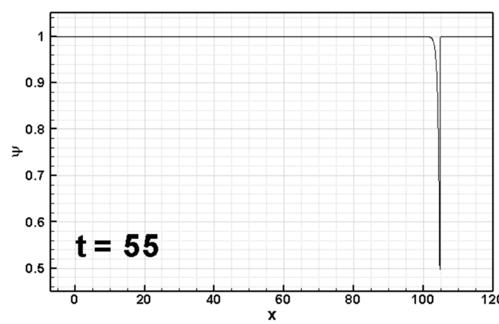

(f) ψ **Variation at** $(t = 55)$

Fig. 11 ψ **Variations at different time steps in a double diaphragm shocktube with diaphragm pressure ratio** $15 : 7 : 1$**.**

its ψ function passes through the relaxation length of the ψ function of the right shock, the ψ value upstream of left shock (from shock reference) is lower than ($\psi_0 = 1$). Therefore its corresponding ψ_{min} will also be lower than its actual value. Therefore, the change in minimum shock function value (ψ_{min}) between $t = 40$ and $t = 48$ shows the passing of left shock function through the relaxation length of right shock function (one instance of this can be seen in figure 11e at $t = 45$). This signifies the need for a smaller relaxation length. The smaller the relaxation length is, the more accurate the ψ variation in the vicinity of two nearby shocks.

Interaction of shock wave and expansion wave

Before the left shock wave meets the right expansion wave head, the flow velocity ahead of the expansion wave is zero ($u_5 = 0$, see figure 10a for station number). When left shock meets the expansion wave head, the velocity ahead of the expansion wave will be u_6. As the shock moves through the expansion wave, the flow velocity is variable, and at a given instant flow velocity immediately ahead of the shock will be, say u_i then flow velocity immediately behind the shock will be $u_i + u_6$, and the velocity variation across the shock should look like the red dash-dot line in figure 13b. Figure 13b superimposes the left shock at two different time instants. At $t = 5$, the left shock is upstream of the right expansion

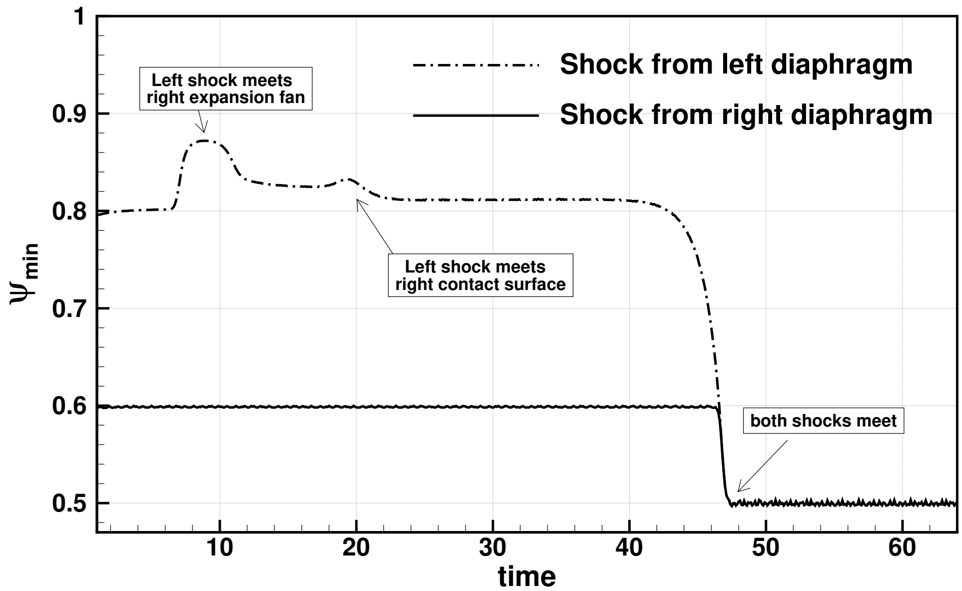

Fig. 12 Variation of minimum ψ for the two shocks with time for the double diaphragm shock tube case with diaphragm pressure ratio $15:7:1$**.**

wave and yet to pass through it. At $y = 8$, the left shock is inside the expansion fan region. The figure is plotted such that the difference of both the velocity (u) axis's maximum and minimum range is the same to match the flow velocity jump across the shock at both the time instants shown by the dash-dot line. (Note that these velocities are with lab reference and do not represent the velocity jump corresponding to the analytical shock relations.) The velocity profile shown by the solid line is the profile simulated using Lax Friedrich's CFD scheme. For the $t = 5$ case, the velocity profile is somewhat closer to the analytical velocity profile; however, for the $t = 8$ case, it is significantly different from the velocity profile analytically. This is because negative dilatation of shock and positive dilatation of expansion fan are both acting at the grid points inside the shock and reducing the net velocity jump across the shock. This, in turn, affects the accuracy of the ψ function when the shock passes through this accelerated flow region. So, the dome seen in ψ_{min} variation in figure 12 is due to this reduced velocity jump across the shock. In reality, the shock strength (ρ_1/ρ_2) and ψ_{min} for the left shock should remain the same until it meets the right shock downstream of it.

Comparisons

Figure 14 shows ψ variation for both left and right shock for the double diaphragm shock tube problem for both original and modified ψ equation for four different length scales: (1) L_ϵ which is variable throughout the domain as well as varies with time, (2) $max(L_\epsilon)$ which is constant throughout the domain but varies with time, (3) multiple of initial $_\epsilon$ $(0.2L_{\epsilon 0} = k_0^{1.5}/\epsilon_0)$ corresponding to M = 1.5 which is the shock Mach number for the right shock and (4) grid size dx.

In figure 14a there is a rise in ψ_{min} value when the first shock passes through the expansion fan and contact surface, which comparatively much higher as compared to the other three cases. This is because L_ϵ is variable throughout the domain and time, and it is maximum at shock and minimum at expansion fan. Because of this, there is a sudden change in L_ϵ value when the shock passes through an expansion fan and contact surface, which directly affects the value of ψ_{min} and the relaxation length. So, to eliminate this effect to some extent, the maximum value of L_ϵ is used as the length scale, and the ψ variation for same is shown in figure 14b. The ψ variation in between $t = 6$ and $t = 25$ is somewhat improved. However, for both the cases ψ_{min} for both the shocks increases slightly with time. This is because L_ϵ and $max(L_\varepsilon)$ change with time and hence the change ψ_{min} value with time. To eliminate the increase in ψ_{min} with time for both the shocks, the initial value of L_ε is used, which is constant throughout the domain as well as with time, and gives almost constant value for shock strength as can be seen in figure 14c. For dx as length scale, similar variation is shock function (ψ) is seen in figure 14d.

The modified equation ($a = 5$ and $b = 30$) clearly provide better result for ψ_{min} value for right shock for all the

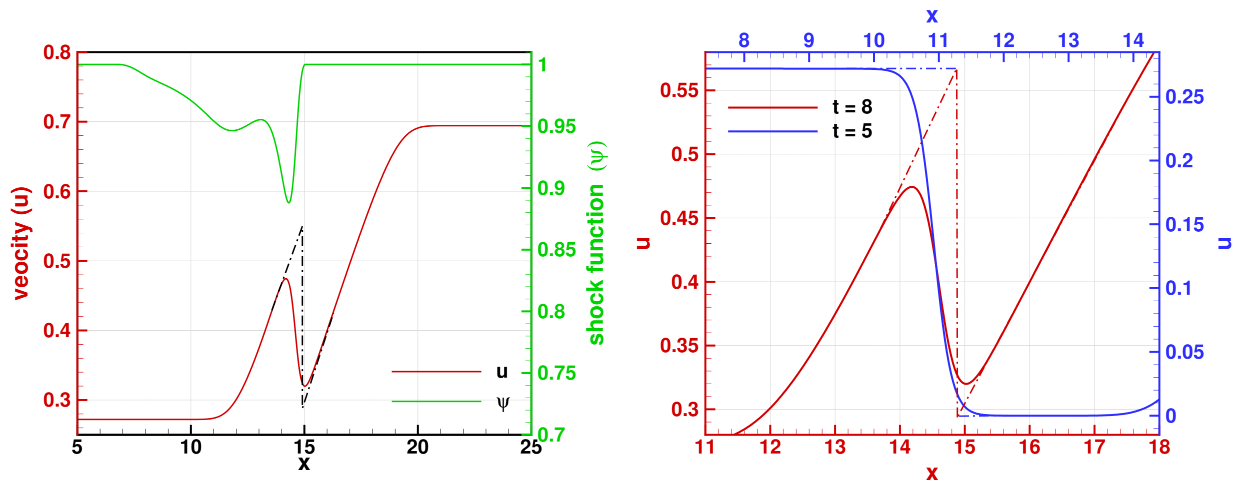

(a) Velocity and ψ variation ($t = 8$).

(b) Superimposed shock locations at $t = 5$ and $t = 8$.

Fig. 13 (a) Velocity and shock function ψ variation when shock passes through expansion fan inside the shock tube and (b) Left shock at two different time instants superimposed over each other. (The dash-dot lines are extrapolated to approximate the analytical location of shock.)

Table 3 Comparison of ψ_{min} results for original and modified ϕ equation for different length scales for a double diaphragm shock tube problem.

		Left shock		Right shock		Combined shock	
		ψ_{min}	$err\%$	ψ_{min}	$err\%$	ψ_{min}	$err\%$
Original ϕ equation	$L = dx$	0.81	5.46	0.62	15.45	0.52	20.93
	$L = L_\epsilon$	0.82	6.77	0.64	19.18	0.52	20.93
	$L = max(L_\epsilon)$	0.8	4.17	0.61	13.59	0.52	20.93
	$L = 0.2L_{\varepsilon_0}$	0.8	4.17	0.6	11.73	0.5	16.27
Modified ϕ equation	$L = dx$	0.79	2.86	0.57	6.14	0.46	6.97
	$L = L_\epsilon$	0.81	5.46	0.59	9.87	0.46	6.97
	$L = max(L_\epsilon)$	0.81	5.46	0.59	9.87	0.46	6.97
	$L = 0.2L_{\epsilon_0}$	0.79	2.86	0.57	6.14	0.46	6.97

cases. However, for left shock, both the equations give very similar results. This is because there is a limit up to which we can reduce the error, after which the results eventually saturate, which is around 3% for the current form of the equation. The quantitative analysis for the ψ_{min} value for different length scales for both original and modified equation is listed in table 3. It can be seen that the error is around 3 to 10% for all three forms of shock.

Comparison with original equation and analytical results for shock Mach number

There are three different velocities associated with a moving shock. Figure 15a shows the schematic for flow across a moving shock from an unsteady or lab frame and a steady or shock frame.
w_1 = Flow velocity ahead of shock
w_2 = Flow velocity behind the shock
u_s = Velocity of the moving shock

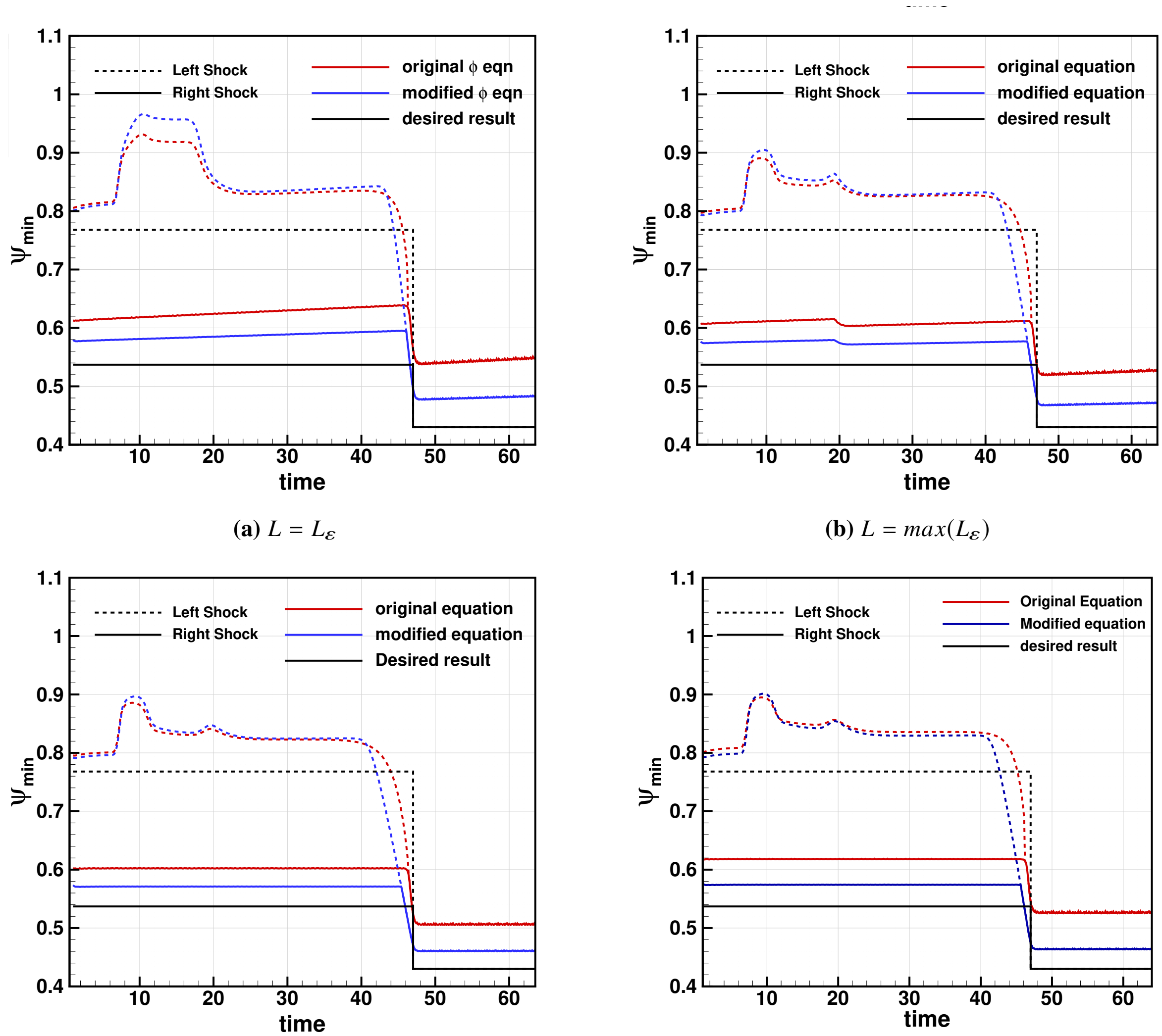

(a) $L = L_\varepsilon$

(b) $L = max(L_\varepsilon)$

(c) $L = 0.2L_{\varepsilon_0}$

(d) $L = 20dx$

Fig. 14 Comparison of modified and original ψ equation results for ψ_{min} for a double diaphragm shock tube problem for diaphragm pressure ratio $15:7:1$ for different Length scales.

The corresponding Mach can be defined as,

$$M_{fx} = \frac{w_1}{a_1}, \qquad M_{fy} = \frac{w_2}{a_2}, \qquad M_{shock} = \frac{u_s}{a_1} \tag{7a}$$

$$M_x = \frac{u_s - w_1}{a_1}, \qquad M_y = \frac{u_s - w_2}{a_2} \tag{7b}$$

where, a_1 and a_2 are speed of sound ahead and behind the shock respectively.

The shock upstream Mach number M_x is calculated using ψ_{min} as density ratio (ρ_1/ρ_2) across the shock and using the corresponding shock relation given by equation 8a.

$$\frac{\rho_2}{\rho_1} = \frac{(\gamma+1)M_x^2}{(\gamma-1)M_x^2+2} \tag{8a}$$

$$\frac{T_2}{T_1} = \frac{\left[2\gamma M_x^2 - (\gamma-1)\right]\left[(\gamma-1)M_x^2+2\right]}{(\gamma+2)^2 M_x^2} \tag{8b}$$

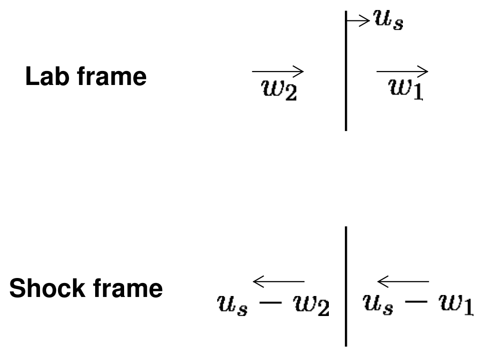

(a) Schematic of moving shock

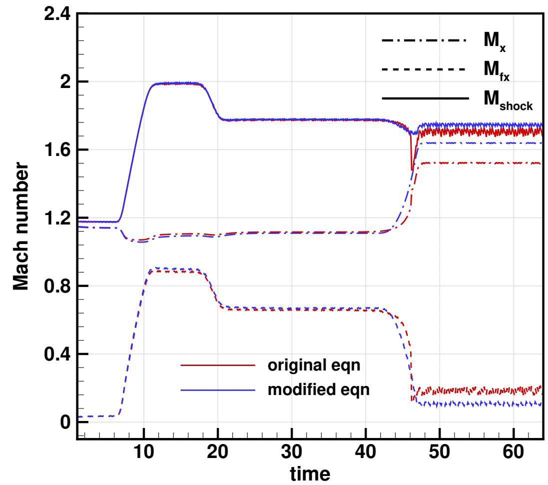

(b) Different Mach number comparison

Fig. 15 (a) Schematic for s moving shock from two different frame of reference and (b) comparison of original and modified equation for different Mach numbers across the left shock for a double diaphragm shock tube problem with diaphragm pressure ratio $15:7:1$**.**

$$M_y^2 = \frac{2 + (\gamma - 1)M_x^2}{2\gamma M_x^2 - (\gamma - 1)} \tag{8c}$$

The flow parameters at the location of ψ_{min}, are the flow parameters just behind the shock. The flow velocity and temperature (w_2 and T_2 respectively) at the location of ψ_{min} are extracted from the simulated results. Using the shock relations (eq. 8) and the Mach number relations (eq. 7), Mach numbers M_{fx} and M_{shock} can be calculated.

Figure 15b shows the variation of the three different Mach numbers M_x, M_{fx} and M_{shock} with time for the left shock for the double diaphragm shock tube problem. It can be seen that left shock Mach number is constant initially and then increase as it passes through the expansion wave because flow Mach number just ahead of the shock (M_{fx}) increases and so does the shock Mach number because $M_{shock} = M_{fx} + M_x$. Left shock M_shock remain constant for some time and then decreases when it passes through the contact discontinuity. This is because flow velocity (w_1) is constant but temperature (T_1) increases across the contact discontinuity and therefore both M_{fx} and M_{shock} decreases. When both the shock meet M_{fx} will be zero and M_x will be equal to M_{shock}. However, M_x and M_{shock} are not exactly equal when both shocks meet because of the oscillations in the extracted values due to computational limitations.

V Conclusion

A shock sensor that identifies both shock location and shock strength in a CFD simulation is introduced by modifying the transport equation for a scalar shock function ψ proposed by Roy et al. [16]. The shock sensor deviates from its reference value in regions of shock waves and the deviation is a measure of the density ratio across the shock. The shock function then relaxes back to its reference value. Two new parameters a and b are included in the original shock function equation to vary the previously constant characteristic length of relaxation. The proposed modification gives better results in terms of shock strength ψ_{min} as well as shock function relaxation length downstream of the shock. The shock sensor is validated for three different cases of stationary shock wave, single diaphragm shock tube, and a double diaphragm shock tube. A grid independence studyfor the stationary shock study shows that for grid size (dx) as characteristic length scale, minimum shock function (ψ_{min}) is independent for almost all grid sizes ranging from a highly coarse to a fine mesh. However, the relaxation length reduces with an increase in the number of grid points. For unsteady cases of the single diaphragm and double diaphragm shock tube, the proposed shock sensor can predict shock location and shock strength accurately. The accuracy of ψ_{min} value depends on the constants a, b and the length scale used. The shock location and strength so estimated can prove useful in estimating the critical regions and flow properties in complex flow simulations with multiple interacting shocks and expansion waves.

References

[1] Pirozzoli, S., "Numerical methods for high-speed flows," *Annual review of fluid mechanics*, Vol. 43, 2011, pp. 163–194.

[2] Shu, C.-W., "Essentially non-oscillatory and weighted essentially non-oscillatory schemes for hyperbolic conservation laws," *Advanced numerical approximation of nonlinear hyperbolic equations*, Springer, 1998, pp. 325–432.

[3] Wu, Z., Xu, Y., Wang, W., and Hu, R., "Review of shock wave detection method in CFD post-processing," *Chinese Journal of Aeronautics*, Vol. 26, No. 3, 2013, pp. 501–513.

[4] Lovely, D., and Haimes, R., "Shock detection from computational fluid dynamics results," *14th Computational Fluid Dynamics Conference*, 1999, p. 3285.

[5] Fujimoto, T. R., Kawasaki, T., and Kitamura, K., "Canny-Edge Detection/ Rankine-Hugoniot conditions unified shock sensor for inviscid and viscous flows," *Journal of Computational Physics*, Vol. 396, 2019, pp. 264–279.

[6] Jameson, A., Schmidt, W., and Turkel, E., "Numerical solution of the Euler equations by finite volume methods using Runge Kutta time stepping schemes," *14th fluid and plasma dynamics conference*, 1981, p. 1259.

[7] Ducros, F., Ferrand, V., Nicoud, F., Weber, C., Darracq, D., Gacherieu, C., and Poinsot, T., "Large-eddy simulation of the shock/turbulence interaction," *Journal of Computational Physics*, Vol. 152, No. 2, 1999, pp. 517–549.

[8] Cockburn, B., Karniadakis, G. E., and Shu, C.-W., "The development of discontinuous Galerkin methods," *Discontinuous Galerkin Methods*, Springer, 2000, pp. 3–50.

[9] Krivodonova, L., Xin, J., Remacle, J.-F., Chevaugeon, N., and Flaherty, J. E., "Shock detection and limiting with discontinuous Galerkin methods for hyperbolic conservation laws," *Applied Numerical Mathematics*, Vol. 48, No. 3-4, 2004, pp. 323–338.

[10] Hill, D. J., and Pullin, D. I., "Hybrid tuned center-difference-WENO method for large eddy simulations in the presence of strong shocks," *Journal of Computational Physics*, Vol. 194, No. 2, 2004, pp. 435–450.

[11] Visbal, M., and Gaitonde, D., "Shock capturing using compact-differencing-based methods," *43rd AIAA Aerospace Sciences Meeting and Exhibit*, 2005, p. 1265.

[12] Kanamori, M., and Suzuki, K., "Shock wave detection in two-dimensional flow based on the theory of characteristics from CFD data," *Journal of Computational Physics*, Vol. 230, No. 8, 2011, pp. 3085–3092.

[13] Lv, Y., See, Y. C., and Ihme, M., "An entropy-residual shock detector for solving conservation laws using high-order discontinuous Galerkin methods," *Journal of Computational Physics*, Vol. 322, 2016, pp. 448–472.

[14] Sinha, K., Mahesh, K., and Candler, G. V., "Modeling shock unsteadiness in shock/turbulence interaction," *Physics of fluids*, Vol. 15, No. 8, 2003, pp. 2290–2297.

[15] Sinha, K., Mahesh, K., and Candler, G. V., "Modeling the effect of shock unsteadiness in shock/turbulent boundary-layer interactions," *AIAA journal*, Vol. 43, No. 3, 2005, pp. 586–594.

[16] Roy, S., Pathak, U., and Sinha, K., "Variable turbulent Prandtl number model for shock/boundary-layer interaction," *AIAA Journal*, Vol. 56, No. 1, 2018, pp. 342–355.

[17] Roy, S., and Sinha, K., "Variable turbulent Prandtl number model applied to hypersonic shock/boundary-layer interactions," *2018 Fluid Dynamics Conference*, 2018, p. 3728.

[18] Jiang, G.-S., and Shu, C.-W., "Efficient implementation of weighted ENO schemes," *Journal of computational physics*, Vol. 126, No. 1, 1996, pp. 202–228.

[19] Jiang, G.-S., and Yu, S.-H., "Discrete shocks for finite difference approximations to scalar conservation laws," *SIAM journal on numerical analysis*, Vol. 35, No. 2, 1998, pp. 749–772.

[20] Larsson, J., and Gustafsson, B., "Stability criteria for hybrid difference methods," *Journal of Computational Physics*, Vol. 227, No. 5, 2008, pp. 2886–2898.

[21] Hendrickson, T. R., Kartha, A., and Candler, G. V., "An improved ducros sensor for the simulation of compressible flows with shocks," *2018 Fluid Dynamics Conference*, 2018, p. 3710.

[22] Ali Pasha, A., and Sinha, K., "Shock-unsteadiness model applied to oblique shock wave/turbulent boundary-layer interaction," *International Journal of Computational Fluid Dynamics*, Vol. 22, No. 8, 2008, pp. 569–582.

[23] Sinha, K., and Balasridhar, S., "Conservative formulation of the $k - \varepsilon$ turbulence model for shock–turbulence interaction," *AIAA journal*, Vol. 51, No. 8, 2013, pp. 1872–1882.

[24] Anderson, J. D., *Modern compressible flow*, Tata McGraw-Hill Education, 2003.